Electronic Supplementary Material

Chlorinated Conjugated Copolymer Interface Modification Enables Record-Efficiency of All-PbS Quantum Dot Tandem Solar Cells

Salman Ali[1], Xinzhao Zhao[2], Mingyu Li[1], Ruiheng Gao[2], Tianjun Ma[1], Yuheng Li[1], Gomaa Mohamed Gomaa Khalaf[3,6], Michael Wang[4], Chris Cheng[4], Jianbing Zhang[5], Ahmed Ghitas[6], Haisheng Song[1,2,7,8,9]✉, and Jiang Tang[1,2,7,8]

[1]*Wuhan National Laboratory for Optoelectronics (WNLO), Huazhong University of Science and Technology (HUST), Wuhan 430074, Hubei, China*

[2]*School of Optical and Electronic Information (SOEI), Huazhong University of Science and Technology (HUST), Wuhan 430074, Hubei, China*

[3]*College of Engineering Physics, Center for Intense Laser Application Technology, Shenzhen Technology University, Shenzhen 518118, Guangdong, China*

[4]*Houston Technology Research Center, CNPC USA Corporation (CNPCUSA), Houston, TX, USA*

[5]*School of Integrated Circuits, Huazhong University of Science and Technology, Wuhan 430074, Hubei, China*

[6]*Solar & Space Research Department, National Research Institute of Astronomy and Geophysics (NRIAG), Egypt*

[7]*Optics Valley Laboratory (OVL), Wuhan 430074, Hubei, China*

[8]*Wenzhou Advanced Manufacturing Technology Research Institute of Huazhong University of Science and Technology, Wenzhou, Zhejiang, PR China*

[9]*Shenzhen R&D Center, Huazhong University of Science and Technology, Shenzhen 518000, P. R. China*

✉Address correspondence to Haisheng Song, songhs-wnlo@mail.hust.edu.cn

1 Experimental

1.1 Chemicals

Zinc stearate ($Zn[CH_3(CH_2)_{16}CO_2]_2$, 99%), lead oxide (PbO, 99.99%), and thioacetamide (C_2H_5NS, 98%) were purchased from Alfa Aesar. Lead chloride ($PbCl_2$, 99.99%), oleic acid (OA, 90%), oleylamine (OLA, 90%), 1-octadecene (ODE, 90%), 1,2-ethanedithiol (EDT, 97%), butylamine (BTA, 98%), octane (98%), and acetone (99.5%) were purchased from Aladdin. Dimethylformamide (DMF, 99.8%), hexane (97%), Ethanol (99.7%), Ethyl acetate (99.7%), acetonitrile (99.8%), chlorobenzene (99.7%), and isopropanol (99.7%) were purchased from Sinopharm. Bis(trimethylsilyl) sulfide (TMS, 97.5%) was purchased from TCI. Indium tin oxide (ITO, 15 $\Omega \cdot sq^{-1}$), lead iodide (PbI_2, 99.99%), and lead bromide ($PbBr_2$, 99.99%) were all purchased from Advanced Election Technology Corp. Self-assembled monolayer (SAMs 4PADCB, 99%) was purchased from Vizuchem. D18-Cl (98%) was purchased from HyperChem.

1.2 QDs Synthesis

We synthesized PbS QDs and fabricated devices from them in the experimental work. We used zinc sulfide (ZnS) QDs (256 nm) as sulfur precursors. The experimental work was as follows: Firstly, we synthesized ZnS QDs, then used them to synthesize PbS QDs at 880 nm and 1300 nm. We used PbS QDs with an exciton peak at 880 nm in the top cell and 1300 nm in the bottom cell to fabricate TSCs.

***ZnS QDs Synthesis*:** For the synthesis of ZnS QDs, 141.2 g of zinc stearate, 7.2 g of thioacetamide, and 560 mL of ODE (1-octadecene) were added to a 2000 mL 2-neck round-bottom flask. Initially, the mixture was stirred and heated to 60 °C for 15 minutes under vacuum. After that, it was filled with nitrogen, and 192 mL of OLA (oleylamine) was added, then heated to 140 °C for 50 minutes. The temperature was reduced to below 70°C, and 64 mL of octylamine was added. The reaction was stopped when the temperature reached 50°C, and the ZnS QDs were washed twice with ethanol at a ratio of 2:3 (ZnS: ethanol) to obtain the ZnS QDs. The QDs were then dispersed in ODE to adjust their concentration.

***PbS QDs 880 nm by cation exchange synthesis method*:** 2 g of $PbCl_2$ (lead chloride) and 24 ml of OLA were added to a 250 ml 3-neck round-bottom flask and heated at 140°C for 35 minutes under vacuum. Then, it was refilled with nitrogen, and the temperature was reduced

to 60 °C. 1.72 g of 0.6 ZnS was added directly through a syringe. The temperature remained constant at 60 °C until the peak was obtained at 880 nm. The heat source was then detached, and 90 ml of hexane and 40 ml of OA (oleic acid) were added to the solution when the temperature dropped below 40 °C, halting the reaction at room temperature. To wash the 880 nm PbS QDs, we used a mixture of ethyl acetate and ethanol (2:3). The QDs were washed twice and centrifuged at 8000 rpm for 3 minutes.

***PbS QDs 1300 nm Synthesis by cation exchange method*:** 2 g of $PbCl_2$ (lead chloride) and 24 mL of OLA were added to a 250 mL 3-neck round-bottom flask and heated at 140°C for 35 minutes under vacuum. It was then refilled with nitrogen, and the temperature was reduced to 60 °C. The ZnS QDs of two different concentrations were added at this temperature using two methods. First, 1.64 g of 0.6 ZnS was added directly through a syringe, followed by the dropwise addition of 0.3 ZnS at a 0.41 mm/min rate. The temperature was gradually increased from 60 to 100 °C over 60 minutes using a temperature-controlled device, then maintained at 100 °C until a peak was observed at 1300 nm. After reaching the desired wavelength peak, 90 mL of hexane and 40 mL of OA (oleic acid) were added to the solution, and the reaction was stopped at room temperature. The QDs were then washed with acetone at a 1:3 (QDs: acetone) ratio, centrifuged at 8000 rpm for 3 minutes, and the supernatant discarded. The remaining desired product adhered to the tube bottoms and walls.

***PbS QDs 880 nm synthesis by TMS method*:** This type of QD was used only as an HTL throughout the devices. To synthesize these QDs, 2.25 g PbO, 20 ml ODE, and 8 ml OA were added to a 250 ml three-neck round-bottom flask and heated at 80 °C for 40 minutes and at 120 °C for another 40 minutes under vacuum. The temperature was then lowered to 100 °C, and the reaction was purged with nitrogen. 700 microliters of TMS were mixed with 5 mL of ODE and added to the reaction. The peak was measured immediately after TMS was added; the reaction was stopped, the heat source was detached, and 20 ml of hexane was added below 70 °C. The reaction was halted at room temperature. The QD solution was stored in the refrigerator overnight and washed after 24 hours using the same cation-exchange method described above for the 880 nm PbS QDs.

1.3 Device Fabrication

***Substrates Cleaning*:** For washing, the 2.5×2.5 cm^2 ITO glass substrates are placed in a sample holder, immersed in a beaker, and sonicated for 30 minutes in water mixed with soap. They are then rinsed for 30 minutes with DI (deionized) water, isopropanol, and ethanol.

***ETL deposition*:** The magnetron sputtering was conducted using a JCP500 high-vacuum multi-target magnetron sputtering system. Zinc oxide (ZnO) with 99.9% purity from Zhongnuo New Material Company was used as the sputtering target. The substrate was maintained at room temperature, and the sputtering power was set to 200 W. A mixed gas of oxygen and argon (O_2: Ar = 1:99) was used as the sputtering gas, with the chamber pressure maintained at approximately 3 Pa throughout the process. The sputtering rate was approximately 2 Å s^{-1}.

***Absorber Layer Deposition*:** For absorber deposition, we first conducted ligand exchange. The PbS QDs (880 nm or 1300 nm) were capped with OA mixed in octane at 10 mg mL^{-1} and then combined with a mixed ligand solution of PbI_2 and $PbBr_2$ in DMF in a 1:1 ratio. This mixture of PbS QDs and ligands was washed three times with octane, then distributed into tubes and centrifuged for 3 minutes at 8000 rpm. The QDs settled to the bottom of the tube, separating from the ligand solvent, and were dried under vacuum in the small chamber of the glove box. For thin-film deposition, the dried QDs were dissolved in a mixed solution of BTA and DMF (4:1) at 130 mg mL^{-1} for top cells and 350 mg mL^{-1} for bottom cells, respectively. The prepared solutions were then spin-coated onto the substrate at 2500 rpm for 40 seconds, followed by drying on a hot plate at 90 °C for 10 minutes. The ligand exchange and thin-film deposition processes were conducted in the glove box under nitrogen.

D18-Cl Deposition: D18-Cl was dissolved in chlorobenzene with variable concentration (0.25-2 mg mL^{-1}) and spin-coated over the PbS-IBr layer at 3000 rpm for 40 seconds in a nitrogen-filled glove box, followed by 10 minutes of annealing at 70 °C.

***HTL Deposition*:** PbS-EDT was used as the HTL. The PbS QD (880 nm) solution in octane at 40 mg mL^{-1} was deposited at 2000 rpm for 20 seconds, followed by a layer of EDT (0.01%), and the sample was washed twice with acetonitrile. This entire process was performed twice. It was conducted in a control room with humidity below 40% and temperature below 30 °C for the top and bottom cells of the TSCs, respectively.

***SAMs Deposition*:** For the interconnection layer, the SAMs solution in ethanol at 0.5 mg mL-1 was spin-coated onto the top cell at 5000 rpm for 30 seconds, with an acceleration of 3000. This process was conducted in a controlled environment with humidity below 40% and a temperature below 30 °C. The samples were subsequently annealed at 100 °C for 10 minutes.

***Au Deposition*:** The 1 nm Au for the recombination layer (RL) and the 70 nm Au for the

back electrode were deposited using e-beam evaporation. The 1 nm Au layer as an RL was deposited at 0.05 Å s^{-1}, while the 70 nm Au layer for the back electrode was deposited at a rate of 0.2 Å s^{-1}.

1.4 Characterization

The current density-voltage (*J-V*) characteristics were measured using a solar simulator (AM 1.5, 100 mW/cm^2) to replicate the solar spectrum. The solar simulator employed a 450 W Oriel Model 9119 Newport xenon lamp. *J-V* curves were collected at a scan rate of 500 mV s^{-1}. Additionally, a monochromatic light source was connected to a quantum efficiency/incident photon-to-electron conversion efficiency (QE/IPCE) mode (QE-R, Enlite Technology) to obtain external quantum efficiency (EQE) spectra. The output spectra were calibrated using a silicon reference cell. To determine the EQE of the tandem cell, the subcells were evaluated under bias conditions that closely matched those of AM 1.5G light. The subcells with narrow and wide band gaps were illuminated with 850 nm and 460 nm laser diodes, respectively.

The chemical compositions of the D18-Cl, PbS-IBr, and PbS-IBr/D18-Cl thin films were analyzed by X-ray photoelectron spectroscopy (XPS) using an AXIS SUPRA+ Shimadzu-Kratos system (Japan). The PbS-IBr and PbS-IBr/D18-Cl thin films' energy levels were examined using ultraviolet photoelectron spectroscopy (UPS) with an AXIS-ULTRA DLD600W system. The work function (Φ) was determined by the difference between the photon energy and the binding energy of the secondary cutoff edge ($\Phi = E_{VAC} - E_F$). The conduction band minimum (EC) was calculated from the optical bandgap, as confirmed by the first exciton absorption peak. Fourier transform infrared spectromicroscopy (FTIR) analysis of the D18-Cl, PbS-IBr, and PbS-IBr/D18-Cl thin films was carried out using a Nicolet iS50R. A Hitachi S-4800 scanning electron microscope (SEM) was used to characterize the film surface and cross-sectional morphology. The surface roughness of the films was investigated using a Jupiter XR atomic force microscope (AFM). Kelvin probe force microscopy (KPFM) in AFM mode was employed to measure the surface potential distribution of the thin films under different conditions.

For photoluminescence (PL) and photoluminescence quantum yield (PLQY) measurements, the samples were excited with an 808 nm laser, and their spectra were recorded using the HORIBA Quanta Master 8000 steady-state transient modular fluorescence spectrometer. The PLQY value was calculated using the appropriate equation, PLQY =

$\frac{J_{\mathrm{rad}}}{J_{\mathrm{rad}}+J_{\mathrm{non-rad}}}$. In the equation, the J_{rad} is the recombination rate, and $J_{\mathrm{non\text{-}rad}}$ is the non-radiative recombination rate of the excited electrons. The quasi-Fermi level splitting (QFLS) values were calculated from the PLQY data using the equation, $QFLS = qV_o^{SQ} + k_bT \ln(PLQY)$. In this equation, the q is the elementary charge, V_o^{SQ} is the theoretical limit of V_{oc} for a specific bandgap, k_{b} is the Boltzmann constant, and T is the temperature. The absorption spectra were obtained using a Solid-Spec 3700 ultraviolet-visible (UV-vis)-near-infrared spectrophotometer.

Capacitance–voltage (*C–V*) measurements were performed with an Agilent 4200A at 100 kHz and an AC signal of 50 mV, scanning from -0.7 V to 0.7 V in 20 mV steps. The V_{bi} were calculated using the equation, $\frac{1}{C^2} = \frac{2(V_{bi}-V)}{A^2 e\, \varepsilon_o \varepsilon_r\, N}$. In this equation, C is the capacitance, V_{bi} is the built-in potential, V is the applied voltage, A is the area of the junction, e is the elementary charge, ε_o is the permitivity of vacuum, ε_r is the relative permitivity of the material, and N is the doping concentration. Electrochemical impedance spectroscopy (EIS) measurements were performed in the dark using a homemade system. A red light-emitting diode (LED, Lumiled) was employed to generate a 1 ms pulse, controlled by a fast solid-state switch. The transient photocurrent was measured with a 40-ohm external series resistance to operate the device under short-circuit conditions. The mobility calculated from the hole-only devices structure (ITO Glass/PEDOT: PSS/PbS-IBr/PbS-EDT/Au and ITO Glass/PEDOT: PSS/PbS-IBr/D18-Cl/PbS-EDT/Au). The mobility is calculated from the equation $J = \frac{9\epsilon_o\epsilon_r\mu V^2}{8L^3}$, ε_{r} is the relative dielectric constant (18 for PbS QDs), ε_{o} is the vacuum permittivity, L is the thickness of the QD films (140 nm), V is the applied voltage, and J is the current density, respectively.

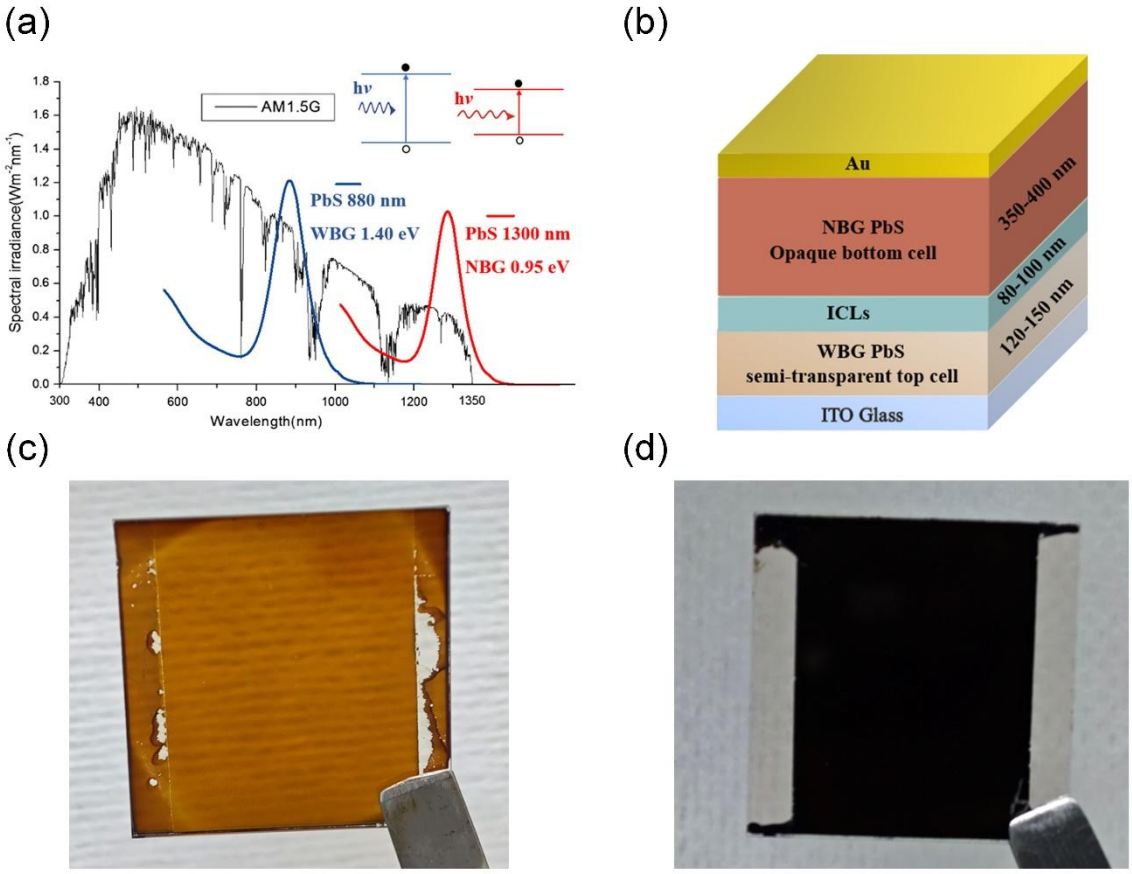

Figure S1. (a) AM 1.5 G standard spectral irradiance distribution overlaid with the absorption peak wavelengths of WBG PbS QDs employed in the top cell and NBG PbS QDs used in the bottom cell of the TSC device, demonstrating complementary spectral coverage. (b) Cross-sectional schematic diagram illustrating the complete tandem device architecture, with layer-by-layer thickness measurements (in nanometers) specified for each functional component of the device stack. (c) Photograph of the fabricated semi-transparent top cell, captured from the glass substrate side, demonstrating partial light transmission. (d) Photograph of the fabricated opaque bottom cell, captured from the glass substrate side, showing complete light absorption.

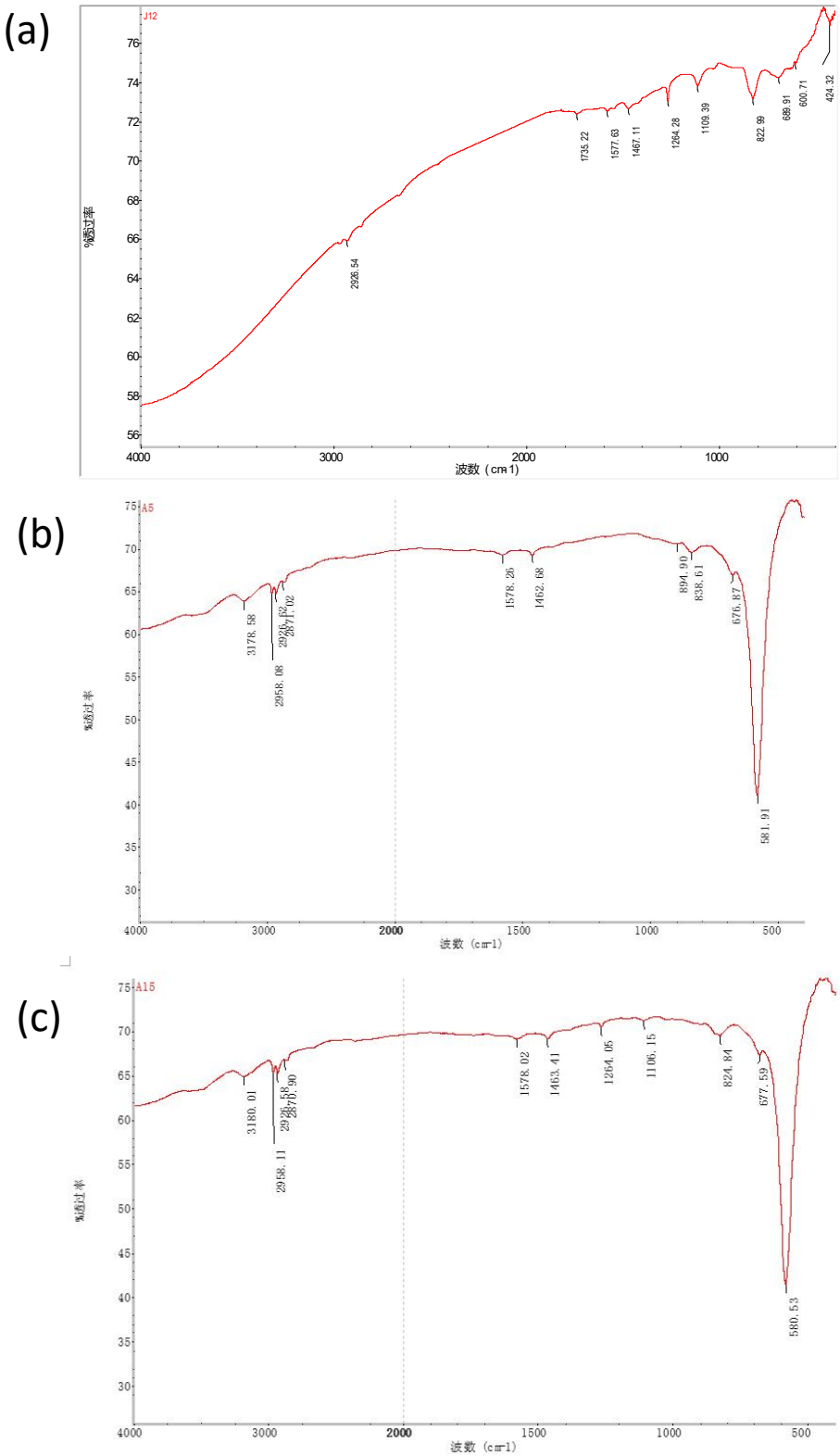

Figure S2. FTIR raw data from the FTIR spectrometer of D18-Cl (a), PbS-IBr (b), and PbS-IBr/D18-Cl (c) thin films

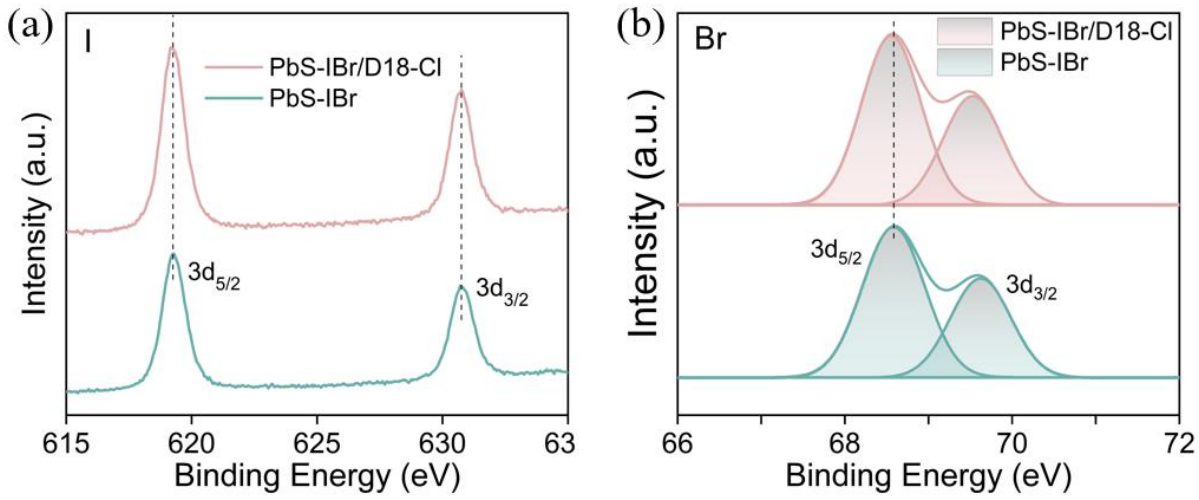

Figure S3. XPS analysis of the PbS-IBr and PbS-IBr/D18-Cl thin films, the elements I (a) and Br (b) binding energies are compared. There is no change in the binding energy of I and Br elements in the pristine and modified thin films, which represents the non-destructive nature of the D18-Cl.

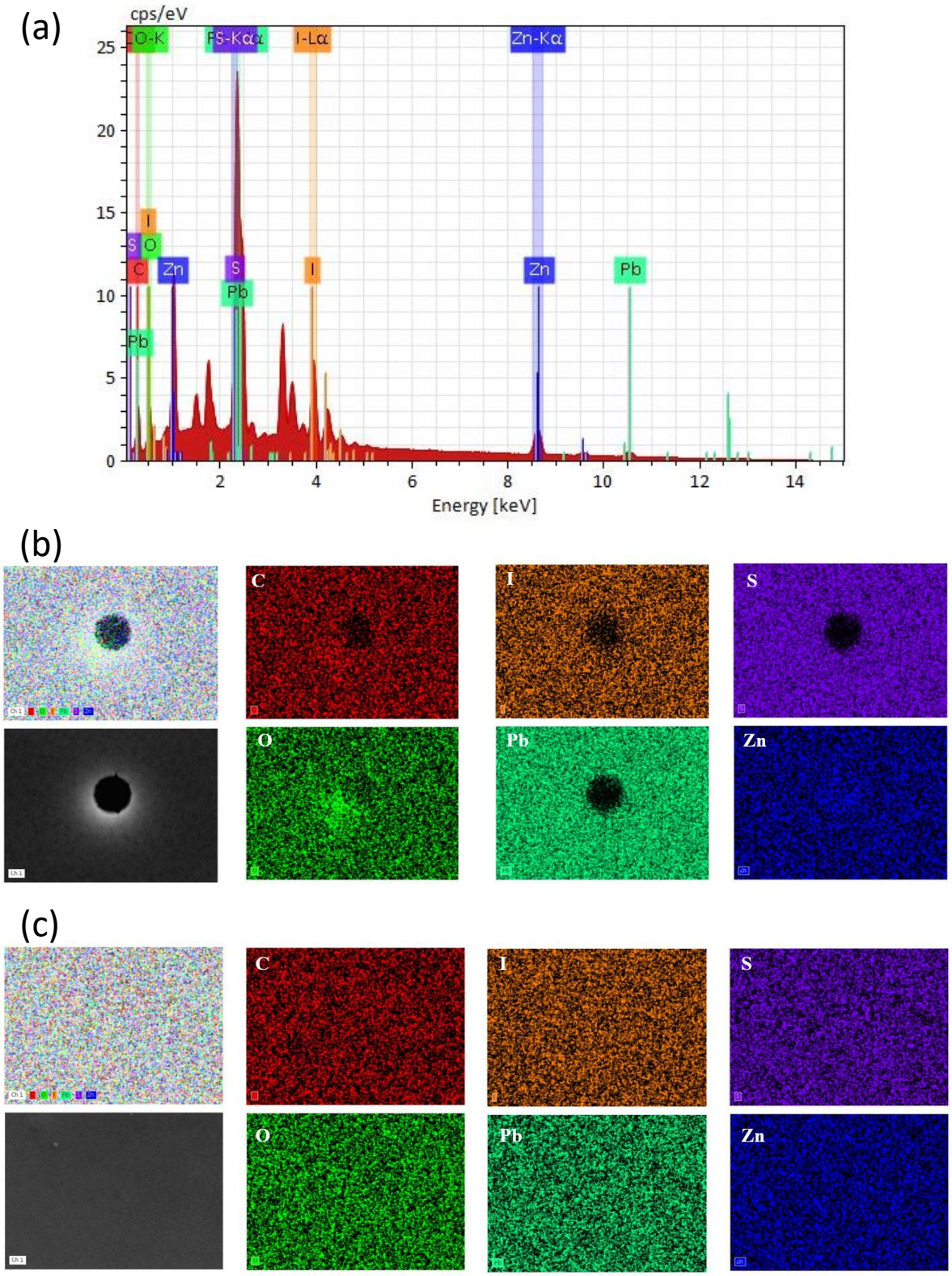

Figure S4. (a) Energy dispersive X-ray (EDX) elemental analysis, (b) elemental map of the PbS-IBr thin film focused on the defective area, and (c) elemental map of the PbS-IBr/D18-Cl thin film.

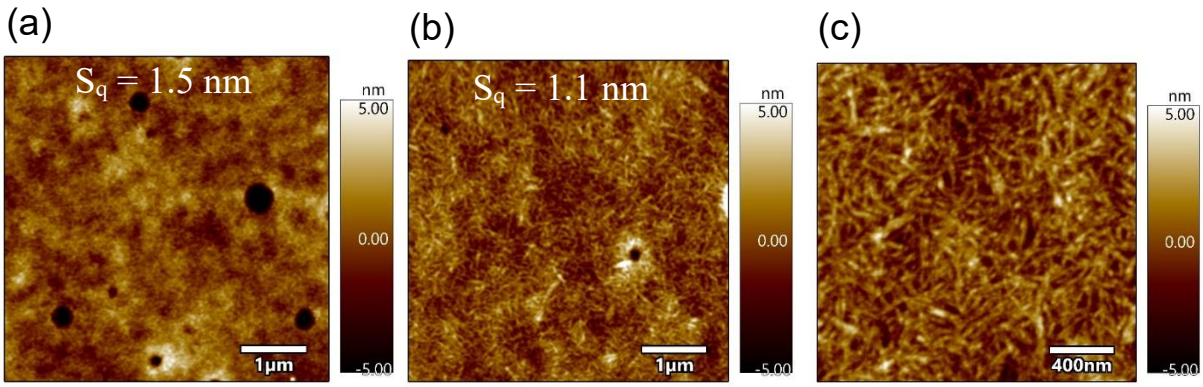

Figure S5. AFM surface analysis images of the PbS-IBr (a) and PbS-IBr/D18-Cl (b) thin films. AFM surface analysis, high magnification images of the PbS-IBr/D18-Cl (c) thin films.

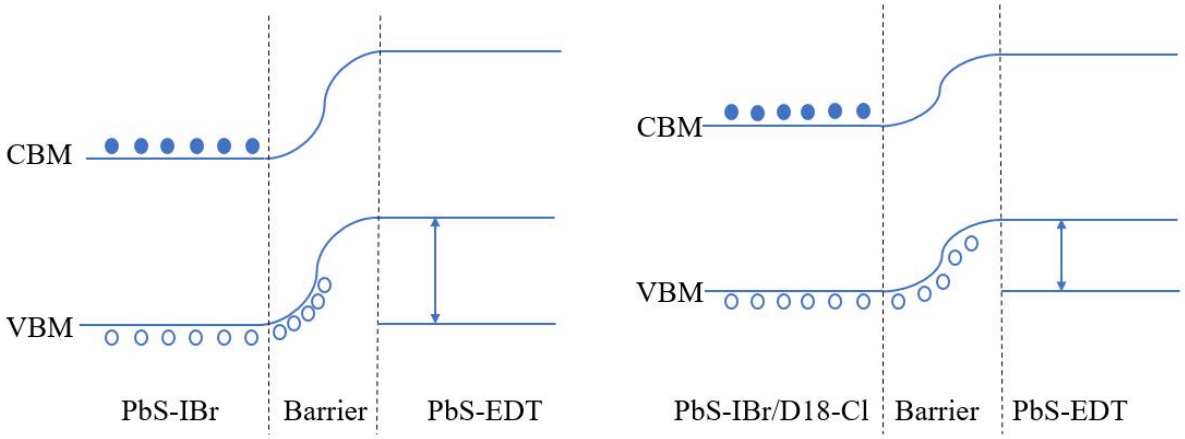

Figure S6. Schematic diagram of the graded pathway for the hole movement. The D18-Cl treatment lowers the energy barrier to hole extraction, enabling more efficient extraction.

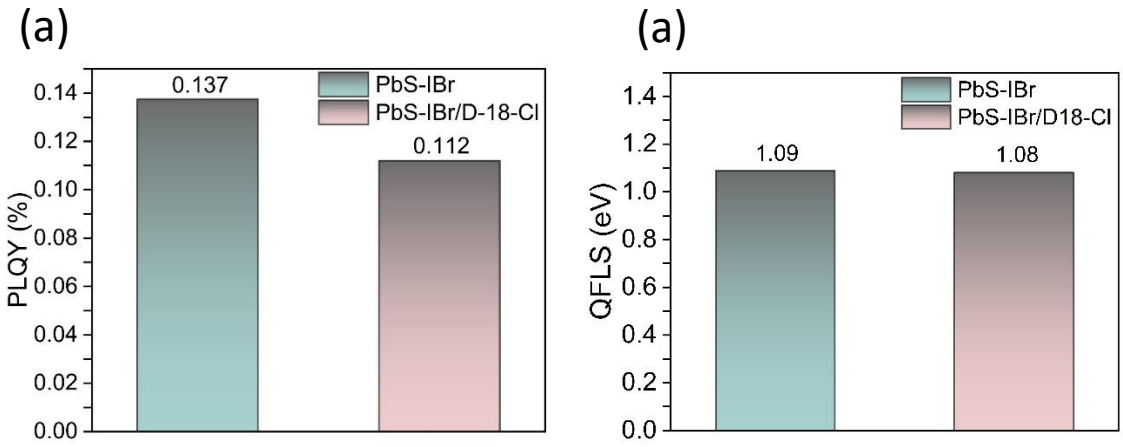

Figure S7. (a) PLQY analysis of the pristine and modified thin films, (b) the QFLS values calculated from the PLQY data.

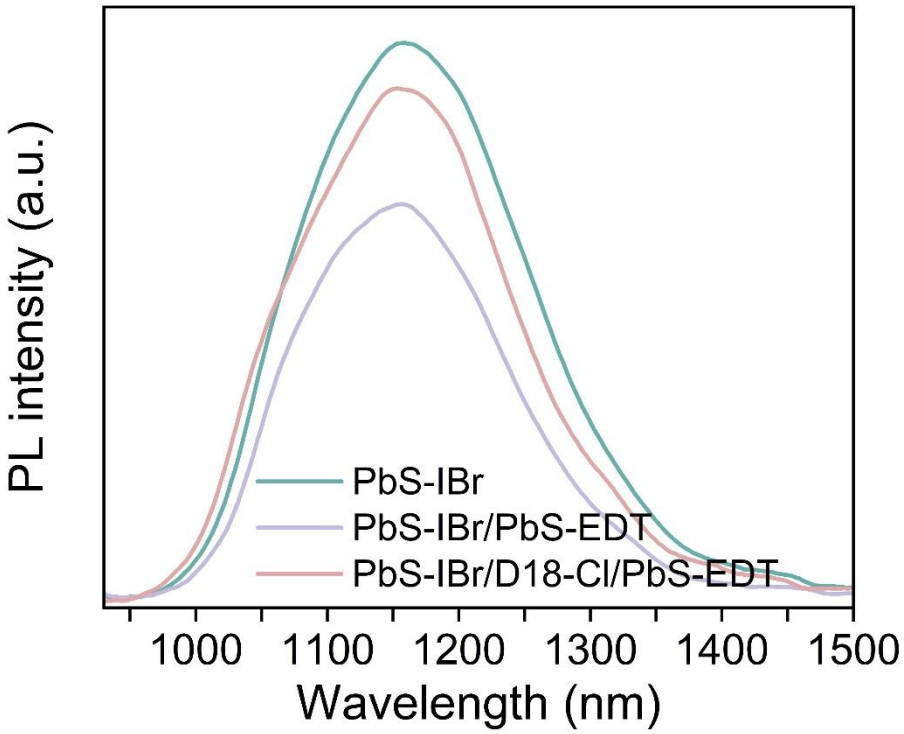

Figure S8. PL spectra of electrode-free complete device stacks (control and D18-Cl-based architectures) compared with the bare PbS absorber layer.

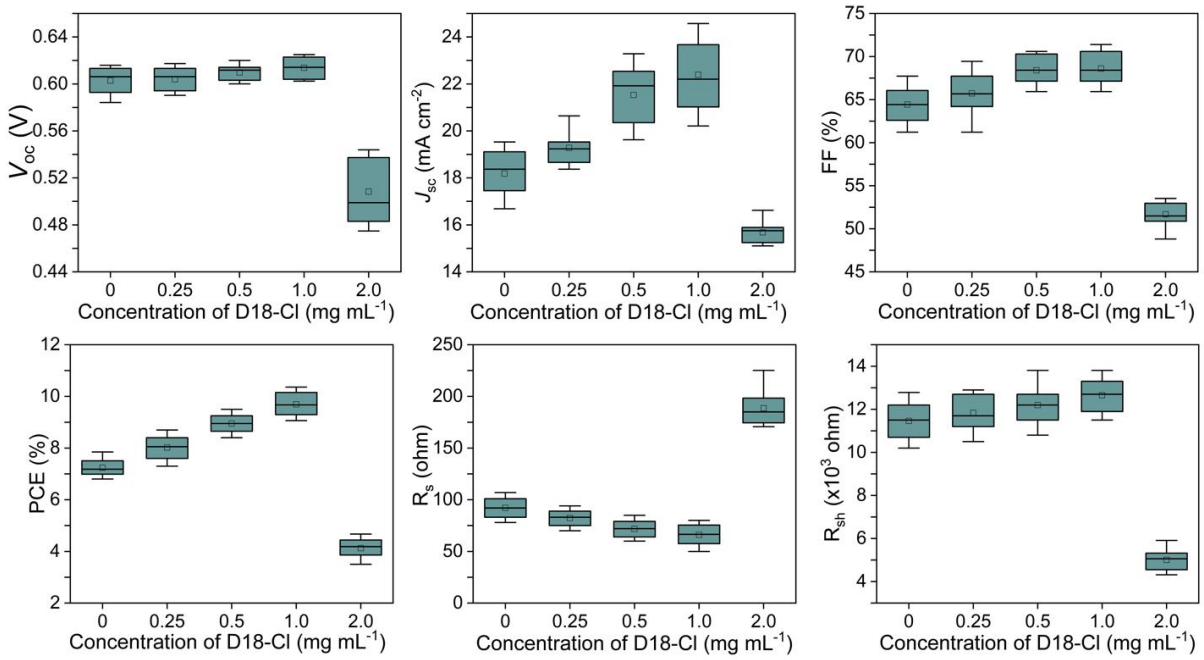

Figure S9. WBG semi-transparent single-junction device performance with varying concentrations of D18-Cl; the 0 mg mL-1 concentration represents the pristine devices, while in the modified devices, the concentration varied from 0 to 2 mg mL^{-1}. An optimum concentration of 1 mg mL^{-1} is selected for the fabrication of all the modified single-junction and tandem devices.

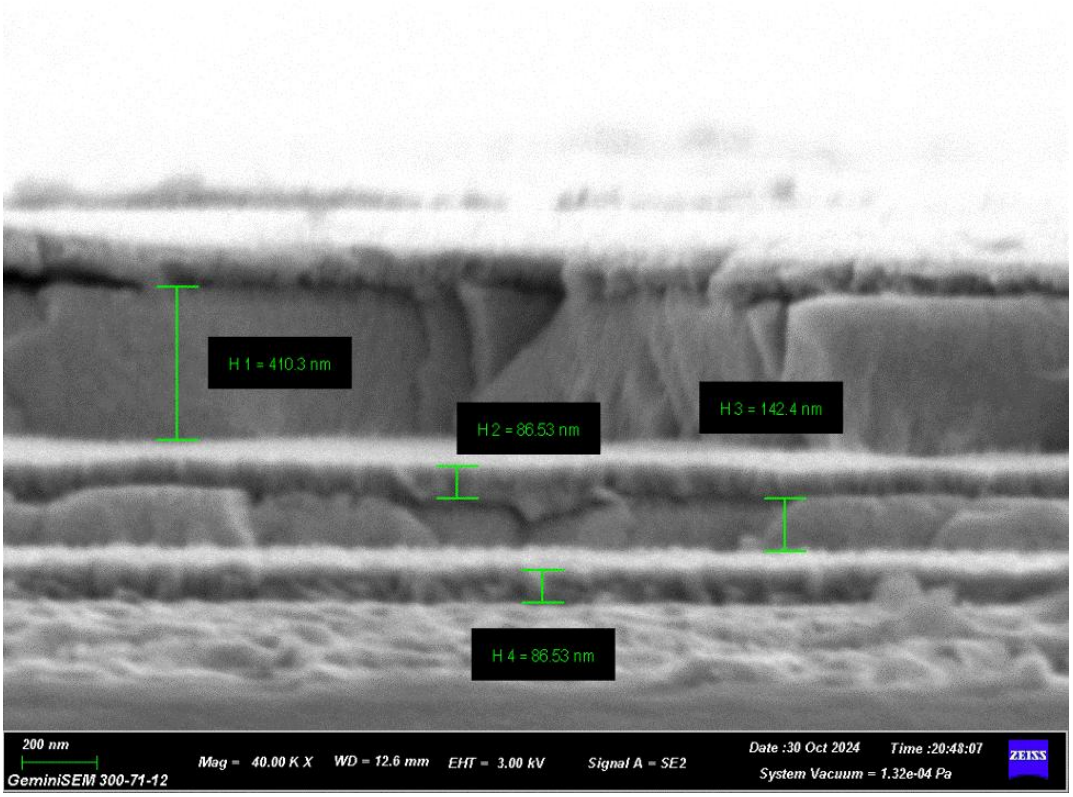

Figure S10. A cross-sectional image of the tandem device displaying a marked thickness of ZnO sputtered onto a glass substrate, along with the top cell absorber, ICL, and bottom cell absorber.

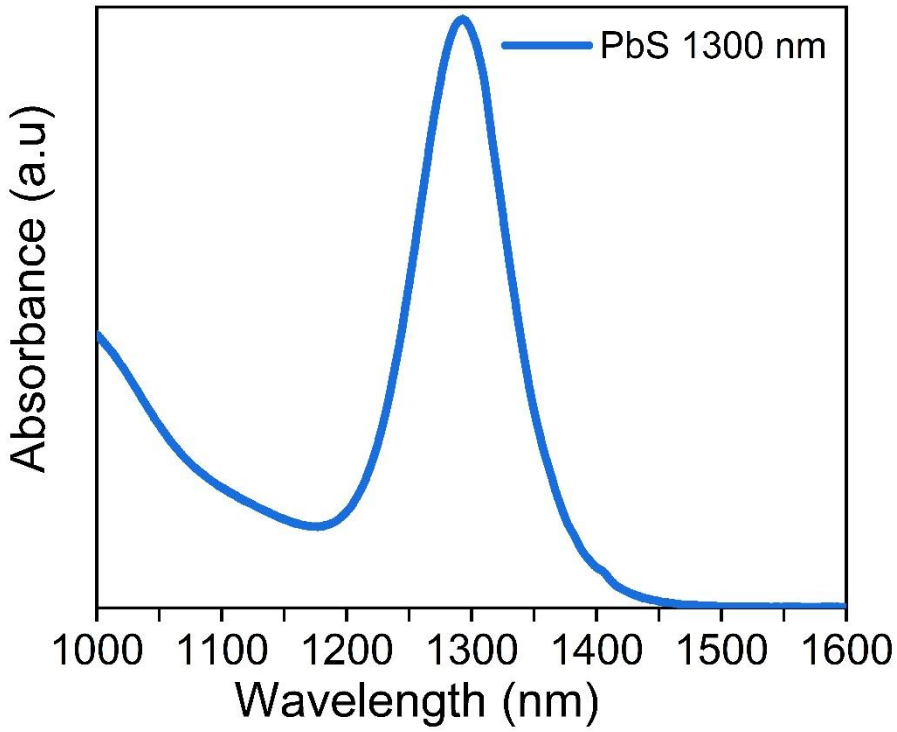

Figure S11. (a) The absorption spectra of PbS 0.95 eV QDs show an intense peak at 1300 nm wavelength.

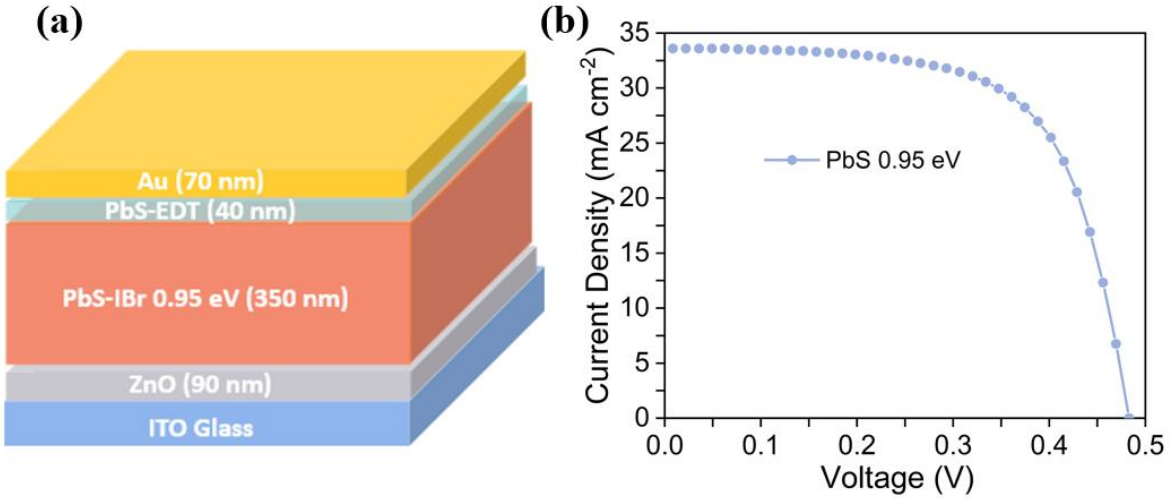

Figure S12. (a) The schematic diagram of the PbS 0.95 eV QDs single junction standard devices, and (b) the *J-V* curve along with the *J-V* parameters.

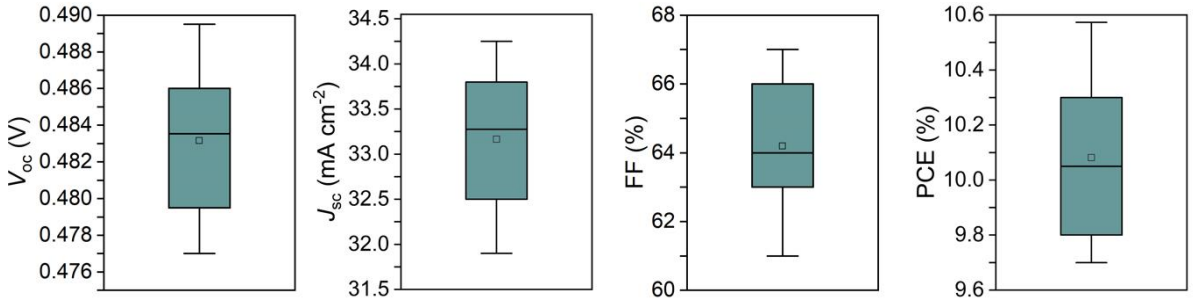

Figure S13. The ranges of the *J-V* parameters for the bottom cell single-junction devices are based on 20 devices.

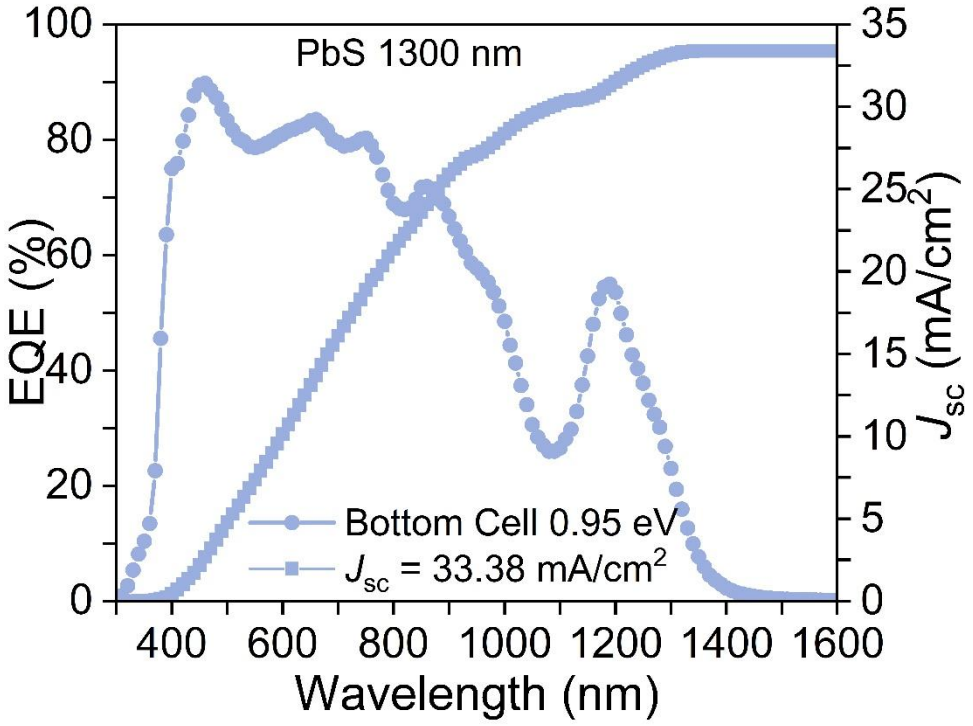

Figure S14. EQE analysis and the calculated integrated J_{sc} for the PbS 0.95 eV single junction standard device.

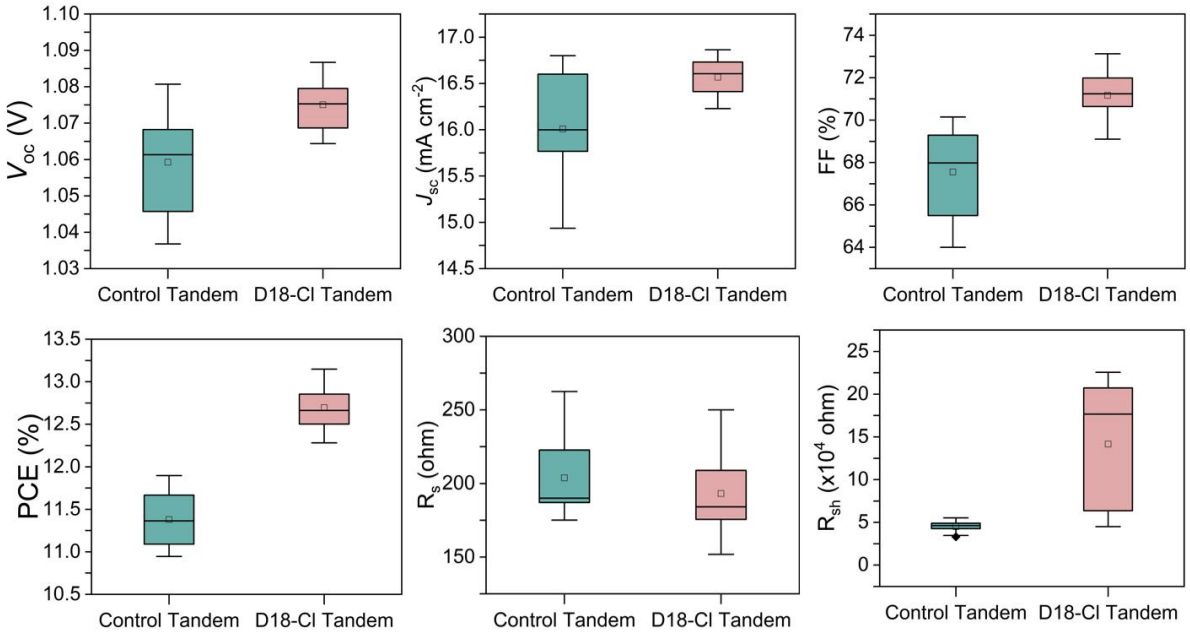

Figure S15. *J-V* parameters for the control and D18-Cl tandem devices. The ranges are based on 20 devices each.

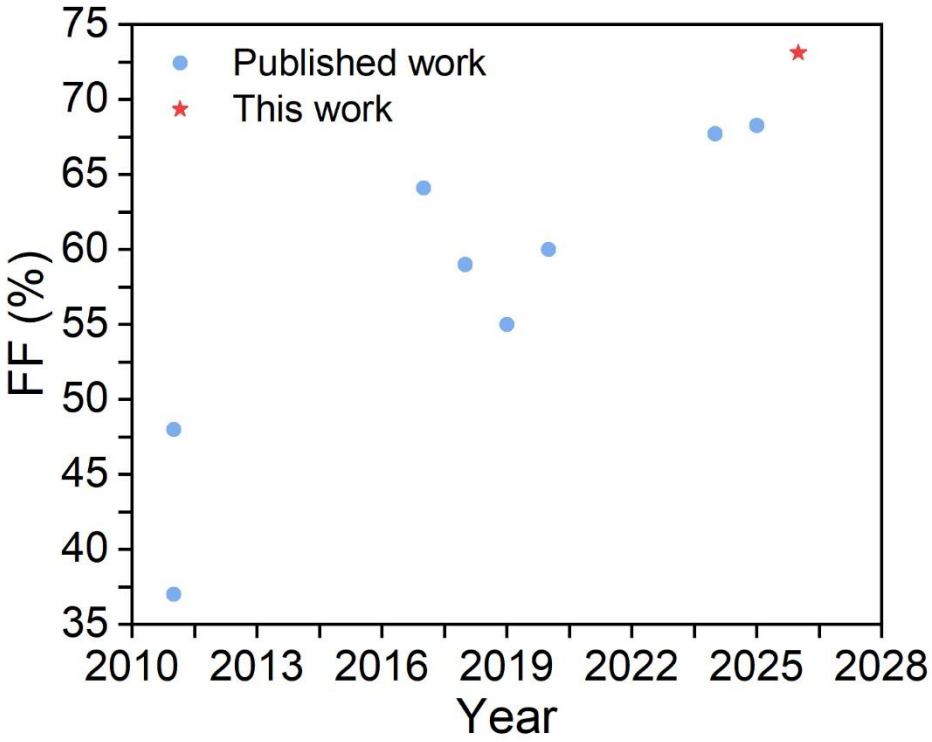

Figure S16: Comparison chart of year-wise FF improvement in the published work compared to this work.

Table S1: Binding energies of the elements detected in the D18-Cl thin film.

20250917\shs-sal\shs-sal\Processed\Quantification

Quantify By: Components

Component	BE [eV]	FWHM [eV]	RSF	Atomic conc. [%]	Error [%]	Mass conc. [%]	Error [%]
S 2p	164.31	1.88	0.67	3.6	0.6	9.0	1.5
Cl 2p	200.96	2.01	0.89	0.8	0.5	2.3	1.4
C 1s	284.96	1.21	0.28	92.8	1.3	85.7	2.2
N 1s	399.56	0.87	0.48	2.8	1.1	3.0	1.2

Table S2: Binding energies of the elements detected in the PbD-IBr thin film.

20250911\shs-sal-xps-1\shs-sal-xps-1\1: Sequence\Processed\Quantification

Quantify By: Components

Component	BE [eV]	FWHM [eV]	RSF	Atomic conc. [%]	Error [%]	Mass conc. [%]	Error [%]
Br 3d	68.65	1.64	1.06	0.7	0.2	0.7	0.2
S 2p	161.25	1.61	0.67	10.4	0.6	3.9	0.2
Cl 2p	193.05	-	0.89	0.0	0.0	0.0	0.0
C 1s	285.00	1.30	0.28	43.1	2.0	6.1	0.5
N 1s	392.60	-	0.48	0.0	-	0.0	-
I 3d	619.30	1.11	10.34	23.8	0.9	35.6	0.7
Pb 4f	138.25	5.77	8.33	22.0	0.8	53.7	0.7

Table S3: Binding energies of the elements detected in the PbS-IBr/D18-Cl thin film

20250911\shs-sal-xps-2\shs-sal-xps-2\1: Sequence\Processed\Quantification

Quantify By: Components

Component	BE [eV]	FWHM [eV]	RSF	Atomic conc. [%]	Error [%]	Mass conc. [%]	Error [%]
Br 3d	68.65	1.67	1.06	0.8	0.3	1.2	0.5
S 2p	161.30	0.82	0.67	10.1	0.9	6.3	0.6
Cl 2p	201.15	0.63	0.89	1.1	0.6	0.7	0.4
C 1s	285.05	1.26	0.28	63.5	1.5	14.8	0.7
N 1s	399.50	0.84	0.48	1.1	0.8	0.3	0.2
I 3d	619.30	1.12	10.34	11.5	0.5	28.4	0.7
Pb 4f	138.15	5.73	8.33	12.0	0.5	48.3	0.9

Table S4: Comparison of the binding energies of thin films detected in the XPS analysis.

S.No:	Element	D18-Cl	PbS-IBr	PbS-IBr/D18-Cl
1	Pb	-	138.25 eV	138.15 eV
2	S	164.31 eV	161.25 eV	161.30 eV
3	I	-	619.30 eV	619.30 eV
4	Br	-	68.65 eV	68.65 eV
5	C	284.96 eV	285.00 eV	285.05 eV
6	Cl	200.96 eV	-	201.15 eV
7	N	399.56 eV	-	399.50 eV

Table S5: Comparison of the WBG PbS top-cell single-junction device performance in all-PbS QD tandem solar cells from the published work with our present work

Year	WBG PbS Top cell bandgap (eV)	Thickness of absorber layer (nm)	V_{OC} (V)	J_{SC} (mA cm^{-2})	FF (%)	PCE (%)
2011	1.60	50	0.58	7.0	44	1.8 [1]
2011	1.60	200	0.7	8.7	49	2.98 [2]
2017	1.33	120	0.58	13.71	63.3	5.3 [3]
2018	1.40	100	0.68	14.50	62.0	6.08 [4]
2019	1.44	190	0.61	12.0	66.0	4.8 [5]
2020	1.45	120	0.66	12.8	64.0	5.4 [6]
2024	1.33	120	0.59	20.8	6.0	7.5 [7]
2025	1.40	140	0.63	18.82	70.2	8.36 [8]
This Work	1.40	140	0.62	24.57	67.47	10.36

Table S6: Comparison of the tandem devices' performance from the published work with our present work devices' performance

Year	Top cell bandgap (eV)	Bottom cell bandgap (eV)	ICLs	V_{OC} (V)	J_{SC} (mA/cm^2)	FF (%)	PCE (%)
2011	1.6	1	ZnO/Au/PEDOT: PSS	0.91	3.7	37	1.27 [1]
2011	1.6	1	MoO_3/ITO/AZO/TiO_2	1.06	8.3	38	4.2 [2]
2017	1.33	1.33	PbS-EDT/Au/ZnO	1.13	12.3	64	8.9 [3]
2018	1.4	0.95	PbS-EDT/Gr/ZnO	0.98	14.58	58	8.2 [4]
2019	1.44	1.22	PbS-EDT/Au/ZnO	1.07	11.5	55	6.8 [5]
2020	1.45	1.22	PbS-EDT/NiO-Ag/ZnO	1.02	11.7	60	7.1 [6]
2024	1.33	0.95	PbS-EDT/PTAA/Au/ZnO	0.91	15.47	67.7	9.5 [7]
2025	1.40	0.95	PbS-EDT/SAMs/Au/ZnO	1.05	16.67	68.3	11.95 [8]
This Work	1.40	0.95	PbS-EDT/SAMs/Au/ZnO	1.07	16.73	73.12	13.148

References

[1] Choi, J. J.; Wenger, W. N.; Hoffman, R. S.; Lim, Y. F.; Luria, J.; Jasieniak, J.; Marohn, J. A.; Hanrath, T. Solution-Processed Nanocrystal Quantum Dot Tandem Solar Cells. *Adv. Mater.* **2011**, *23*, 3144–3148.

[2] Wang, X.; Koleilat, G. I.; Tang, J.; Liu, H.; Kramer, I. J.; Debnath, R.; Brzozowski, L.; Barkhouse, D. A. R.; Levina, L.; Hoogland, S.; Sargent, E. H. Tandem Colloidal Quantum Dot Solar Cells Employing a Graded Recombination Layer. *Nat. Photonics* **2011**, *5*, 480–484.

[3] Shi, G.; Wang, Y.; Liu, Z.; Han, L.; Liu, J.; Wang, Y.; Lu, K.; Chen, S.; Ling, X.; Li, Y.; Cheng, S.; Ma, W. Stable and Highly Efficient PbS Quantum Dot Tandem Solar Cells Employing a Rationally Designed Recombination Layer. *Adv. Energy Mater.* **2017**, *7*, 1602667.

[4] Bi, Y.; Pradhan, S.; Akgul, M. Z.; Gupta, S.; Stavrinadis, A.; Wang, J.; Konstantatos, G. Colloidal Quantum Dot Tandem Solar Cells Using Chemical Vapor Deposited Graphene as an Atomically Thin Intermediate Recombination Layer. *ACS Energy Lett.* **2018**, *3*, 1753–1759.

[5] Gao, Y.; Zheng, J.; Chen, W.; Yuan, L.; Teh, Z. L.; Yang, J.; Cui, X.; Conibeer, G.; Patterson, R.; Huang, S. Enhancing PbS Colloidal Quantum Dot Tandem Solar Cell Performance by Graded Band Alignment. *J. Phys. Chem. Lett.* **2019**, *10*, 5729–5734.

[6] Hu, L.; Wang, Y.; Shivarudraiah, S. B.; Yuan, J.; Guan, X.; Geng, X.; Younis, A.; Hu, Y.; Huang, S.; Wu, T.; Halpert, J. E. Quantum-Dot Tandem Solar Cells Based on a Solution-Processed Nanoparticle Intermediate Layer. *ACS Appl. Mater. Interfaces* **2020**, *12*, 2313–2318.

[7] Mohamed Gomaa Khalaf, G.; Zhao, X.; Li, M.; Li, C.; Ali, S.; Ma, T.; Hsu, H. Y.; Zhang, J.; Song, H. Efficient PbS Quantum Dots Tandem Solar Cells through Compatible Interconnection Layer. *Journal of Energy Chemistry* **2024**, *98*, 47–57.

[8] Ali, S.; Khalaf, G. M. G.; Ke, A.; Li, C.; Zhao, X.; Shen, G.; Yan, J.; Ishaq, M.; Hsu, H. Y.; Chen, C.; Zhang, J.; Song, H.; Tang, J. Interface Modification Enables 11.95%-Efficient All-PbS-QDs Tandem Solar Cells Utilizing Self-Assembled Monolayers. *Solar RRL* **2025**, *9* (24).